SPICE: A Sparsity Promoting Iterated Constrained Endmember Extraction Algorithm with Applications to Landmine Detection from Hyperspectral Imagery

Alina Zare and Paul Gader
University of Florida, CISE Building, Gainesville, FL 32611-6120 USA

ABSTRACT

An extension of the Iterated Constrained Endmembers (ICE) algorithm that incorporates sparsity promoting priors to find the correct number of endmembers is presented. In addition to solving for endmembers and endmember fractional maps, this algorithm attempts to autonomously determine the number of endmembers required for a particular scene. The number of endmembers is found by adding a sparsity-promoting term to ICE's objective function. This method is applied to long wave infrared, LWIR, hyperspectral data to seek out vegetation endmembers and define a vegetation mask for the reduction of false alarms in landmine data.

Keywords: Sparsity Promotion, Endmember, Hyperspectral Imagery

1. INTRODUCTION

Autonomous endmember detection is a difficult problem in hyperspectral imaging. Many endmember extraction algorithms have been formulated but the majority of these algorithms require the knowledge of the number of endmembers required for a scene. The problem of autonomously determining the number of required endmembers to a large extent has not been tackled.

We provide an extension of the Iterated Constrained Endmembers (ICE) Algorithm[1] that provides better estimates of the number of endmembers required for a dataset. This extension adds a sparsity-promoting term to the ICE objective function and is, therefore, referred to as SPICE. This added term encourages the pruning of unnecessary endmembers.

In Section 2, we review the ICE algorithm and discuss the sparsity promoting extension. It is assumed that the reader is familiar with the endmember detection problem. In Section III, we present results on real image data with application to false alarm reduction for landmine detection. Section IV is the conclusion.

2. ICE WITH SPARSITY PROMOTION

2.1 Review of ICE algorithm

The ICE Algorithm performs a least squares minimization of the residual sum of squares (RSS) based on the convex geometry model. The convex geometry model assumes that every pixel in a scene is a linear combination of the endmembers of the scene. The convex geometry model can be written as

$$\mathbf{X}_i = \sum_{k=1}^{M} p_{ik}\mathbf{E}_k + \varepsilon_i \qquad i = 1,\ldots, N \tag{1}$$

where N is the number of pixels in the image, M is the number of endmembers, ε_i is an error term, p_{ik} is the proportion of endmember k in pixel i, and $\mathbf{E}_k$ is the k^{th} endmember. The proportions satisfy the constraints

$$p_{ik} \geq 0, k = 1,\ldots.M, \qquad \sum_{k=1}^{M} p_{ik} = 1. \tag{2}$$

Detection and Remediation Technologies for Mines and Minelike Targets XII
edited by Russell S. Harmon, J. Thomas Broach, John H. Holloway, Jr.
Proc. of SPIE Vol. 6553, 655319, (2007) · 0277-786X/07/$18 · doi: 10.1117/12.722595

By minimizing the RSS, subjected to the constraints in (2), the error between the pixel spectra and the pixel estimate found by the ICE algorithm for the endmembers and their proportions is minimized.

$$RSS = \sum_{i=1}^{N} \left(\mathbf{X}_i - \sum_{k=1}^{M} p_{ik} \mathbf{E}_k \right)^T \left(\mathbf{X}_i - \sum_{k=1}^{M} p_{ik} \mathbf{E}_k \right) \tag{3}$$

As described in reference 1, the minimizer for RSS is not unique. Therefore, the ICE algorithm adds a sum of squared distances (SSD) term to the objective function.

$$SSD = \sum_{k=1}^{M-1} \sum_{l=k+1}^{M} (\mathbf{E}_k - \mathbf{E}_l)^T (\mathbf{E}_k - \mathbf{E}_l) \tag{4}$$

This term is proportional to the size of the area bounded by the endmembers. Therefore, by adding this term to the objective function, the algorithm finds endmembers that provide a tight fit around the data. In reference 1, it is shown that SSD is equivalent to

$$SSD = M(M-1)V \tag{5}$$

where V is the sum of variances (over the bands) of the simplex vertices. As done in reference 1, V is used in the objective function instead of $M(M-1)V$ in an effort to make this term independent of the number of endmembers, M. Therefore, the objective function used in the ICE algorithm is

$$RSS_{reg} = (1-\mu)\frac{RSS}{N} + \mu V \tag{6}$$

where μ is the regularization parameter that balances the RSS and SSD terms of the objective function.

The ICE algorithm minimizes this objective function iteratively. First, given endmember estimates, the proportions for each pixel are estimated. For the first iteration of the algorithm, endmember estimates may be set to randomly chosen pixels from the image. This requires a least squares minimization of each term in (3). Since each of these terms is quadratic and subjected to the linear constraints in (2), the minimization is done using quadratic programming. After solving for the proportions, the endmembers are found using the current proportion estimates:

$$\mathbf{e}_j = \left\{ \mathbf{P}^T \mathbf{P} + \lambda \left(\mathbf{I}_M - \frac{\mathbf{1}\mathbf{1}^T}{M} \right) \right\}^{-1} \mathbf{P}^T x_j \tag{7}$$

where $\mathbf{P}$ is the N x M proportion matrix, $\mathbf{e}_j$ is the vector of endmember values in the j*th* band, $\mathbf{x}_j$ is the vector of all the pixel values in the j*th* band, $\mathbf{I}_M$ is the M x M identity matrix, $\mathbf{1}$ is the M-vector of ones and $\lambda = N\mu/\{(M-1)(1-\mu)\}$. This iterative procedure is continued until the value of RSS_{reg} is smaller than a tolerance value. Although the ICE algorithm is an excellent algorithm for finding endmembers when the number of endmembers is known, there is no automated mechanism in ICE to determine the correct number of endmembers. Our proposed extension uses sparsity promoting priors to alleviate this disadvantage.

2.2 Sparsity Promotion

The RSS term of the objective function is a least squares term whose minimization is equivalent to the maximization[2] of

$$-\frac{1}{2}\sum_{i=1}^{N}\left(\mathbf{x_i}-\sum_{k=1}^{M}p_{ik}\mathbf{E}_k\right)^2=\ln e^{-\frac{1}{2}\sum_{i=1}^{N}\left(\mathbf{x_i}-\sum_{k=1}^{M}p_{ik}\mathbf{E}_k\right)^2}. \tag{8}$$

When examining the exponential in (8), it can be seen that this is proportional to the Gaussian density with mean $\sum_{k=1}^{M}p_{ik}\mathbf{E}_k$ and variance 1.

$$N(\sum_{k=1}^{M}p_{ik}\mathbf{E}_k,1)=\frac{1}{\sqrt{2\pi}}e^{-\frac{\sum_{i=1}^{N}\left(\mathbf{x_i}-\sum_{k=1}^{M}p_{ik}\mathbf{E}_k\right)^2}{2}}\propto e^{-\frac{1}{2}\sum_{i=1}^{N}\left(\mathbf{x_i}-\sum_{k=1}^{M}p_{ik}\mathbf{E}_k\right)^2} \tag{9}$$

A common method to promote small parameter values during a least squares minimization process is to add a weight decay term to the objective function. The weight decay term attempts to prevent the p_{ik} values from becoming large.

$$\begin{aligned}LSWD&=\ln e^{-\frac{1}{2}\sum_{i=1}^{N}\left(\mathbf{x_i}-\sum_{k=1}^{M}p_{ik}\mathbf{E}_k\right)^2-\gamma\sum_{i=1}^{N}\sum_{k=1}^{M}p_{ik}^2}\\&=\ln\left[e^{-\frac{1}{2}\sum_{i=1}^{N}\left(\mathbf{x_i}-\sum_{k=1}^{M}p_{ik}\mathbf{E}_k\right)^2}e^{-\gamma\sum_{i=1}^{N}\sum_{k=1}^{M}p_{ik}^2}\right]\end{aligned} \tag{10}$$

where $\gamma\geq 0$. The second exponential in (10) can also be seen as a Gaussian with a mean of zero. Therefore, (10) can be viewed as the log of the following product.

$$p(\mathbf{X}\,|\,\mathbf{P})\,p(\mathbf{P}) \tag{11}$$

where $p(\mathbf{X}\,|\,\mathbf{P})$ is the probability of the data given the parameters and $p(\mathbf{P})$ is the prior on the parameters.

Unfortunately, the Gaussian prior is not effective at sparsity promotion. The Gaussian does not prefer to set parameter values to zero which would promote sparsity; instead the Gaussian prefers several small valued non-zero parameters. Therefore, instead of using a Gaussian distribution for the parameters' prior, a zero-mean Laplacian distribution can be used to promote sparsity [3].

$$LSSP=-\frac{1}{2}\sum_{i=1}^{N}\left(\mathbf{x_i}-\sum_{k=1}^{M}p_{ik}\mathbf{E}_k\right)^2-\sum_{k=1}^{M}\gamma_k\sum_{i=1}^{N}|p_{ik}| \tag{12}$$

2.3 Sparsity Promoting Iterated Constrained Endmembers

Given equation (12), we see that the sparsity promoting term should be of the form:

$$SPT=\sum_{k=1}^{M}\gamma_k\sum_{i=1}^{N}|p_{ik}|=\sum_{k=1}^{M}\gamma_k\sum_{i=1}^{N}p_{ik} \tag{13}$$

where the last equality follows due to the constraints in (2). For this work, we take

$$\gamma_k = \frac{\Gamma}{\sum_{i=1}^{N} p_{ik}}. \tag{14}$$

Γ is a constant associated with the degree that the proportion values are driven to zero. The advantage of this expression for γ_k is that as the proportion values change during the minimization of the objective function, the weight associated with each endmember adjusts accordingly. If the sum of a particular endmember's proportion values becomes small, then the weight, γ_k, for that endmember becomes larger. This weight change accelerates the minimization of those proportion values. Furthermore, since the objective function is minimized in an iterative fashion, the change in the γ_k values does not disrupt the minimization.

Incorporating this new term into ICE's objective function yields

$$RSS^*_{reg} = (1-\mu)\frac{RSS}{N} + \mu V + SPT \tag{15}$$

This can be rewritten as

$$\begin{aligned} RSS^*_{reg} &= \frac{(1-\mu)}{N}\sum_{i=1}^{N}\left(\mathbf{X}_i - \sum_{k=1}^{M} p_{ik}\mathbf{E}_k\right)^T\left(\mathbf{X}_i - \sum_{k=1}^{M} p_{ik}\mathbf{E}_k\right) + \mu V + \sum_{k=1}^{M}\gamma_k\sum_{i=1}^{N} p_{ik} \\ &= \frac{(1-\mu)}{N}\sum_{i=1}^{N}\left[\left(\mathbf{X}_i - \sum_{k=1}^{M} p_{ik}\mathbf{E}_k\right)^T\left(\mathbf{X}_i - \sum_{k=1}^{M} p_{ik}\mathbf{E}_k\right) + \frac{N}{(1-\mu)}\sum_{k=1}^{M}\gamma_k p_{ik}\right] + \mu V \end{aligned} \tag{16}$$

In order to minimize this new objective function, the iterative procedure used in ICE can still be used. The endmembers are still found by solving (7) since SPT does not depend on the endmembers. When solving for the proportion values given endmember estimates, each of the N terms of the following sum need to be minimized given the constraints in (2) using quadratic programming.

$$RSS^*_{reg,term1} = \frac{(1-\mu)}{N}\sum_{i=1}^{N}\left[\left(\mathbf{X}_i - \sum_{k=1}^{M} p_{ik}\mathbf{E}_k\right)^T\left(\mathbf{X}_i - \sum_{k=1}^{M} p_{ik}\mathbf{E}_k\right) + \sum_{k=1}^{M}\gamma^*_k p_{ik}\right] \tag{17}$$

where

$$\gamma^*_k = \frac{\Gamma^*}{\sum_{i=1}^{N} p_{ik}}, \quad \Gamma^* = \frac{N\Gamma}{(1-\mu)} \tag{18}$$

During the iterative minimization process, endmembers can be pruned as their proportion values drop below a pruning threshold. After every iteration of the minimization process, the maximum proportion values for every endmember can be calculated.

$$MAXP_k = \max_i\{p_{ik}\} \tag{19}$$

If the maximum proportion for an endmember drops below a threshold, then the endmember can be pruned from the endmember set.

3. EXPERIMENTS AND RESULTS

3.1 Data

The SPICE algorithm was run on data collected by AHI, the Airborne Hyperspectral Imager[4]. AHI collects 256 spectral bands of data from the long wave infrared region in the range of 7.88 to 11.49 microns. The data collected is trimmed and binned down to 70 bands over the save wavelengths. The data set used in this paper was collected from an arid

testing site containing both surface and buried landmines. Fiducial markers are also contained in the imagery for alignment and ground truthing purposes.

Three AHI images were used for this study. Scoring for the results in this paper was done over regions of interest in the imagery. The regions of interest for this study were defined as the areas where collected Lynx Synthetic Aperture Radar[5] and AHI imagery intersect. Four mine types were distributed in the overlap regions. Two of the mine types were plastic cased (PC) and two were metal cased (MC). The distribution of mines types in the overlap regions of these three images are displayed in Table 1.

Table 1. Mine Distributions in Overlap Regions

		AHI Image 1	AHI Image 2	AHI Image 3
Mine Type	**Depth**	**Quantity**	**Quantity**	**Quantity**
PC1	10 cm	44	17	17
MC1	10 cm	57	48	26
MC1	Flush	34	34	20
MC1	Surface	16	16	16
MC2	Surface	14	14	0
PC2	Surface	5	0	0
Total		**170**	**129**	**79**

Figure 1 displays a subset of AHI Image 2 at 9.19 microns. At this wavelength, the vegetation appears dark in the imagery. Additionally, buried mines can be seen in a grid throughout the image.

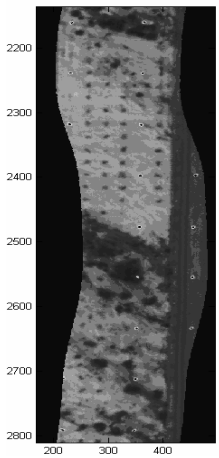

Figure 1: Subset of AHI Image 2 including overlap region at 9.19 microns.

3.2 Vegetation mapping

Vegetation detection in the LWIR is based on the emissive properties of vegetation. Vegetation behaves similar to a blackbody in the LWIR exhibiting a high mean emissivity and a low standard deviation of emissivity across spectral bands[5]. Additionally, as described in reference 7, skewness of emissivity across spectral bands has been seen to be helpful in distinguishing vegetation. To exploit this information, the SPICE algorithm can be run on the emissivity spectra calculated from LWIR hyperspectral data. For this study, the emissivity spectrum of each pixel in the image is calculated using the Emissivity Normalization Method[8].

After applying the SPICE algorithm to the emissivity spectra, the endmembers determined by the algorithm are examined. The endmember with the highest mean and the lowest standard deviation is determined to be the blackbody endmember.

$$E_B = \begin{cases} E_i & if \ \arg\max_{E_i}(\mu_i) = \arg\min_{E_i}(\sigma_i) \\ \varnothing & otherwise \end{cases} \tag{20}$$

where μ_i is the mean and σ_i is the standard deviation across spectral bands of the i^{th} endmember, E_i, found by SPICE.

Since the proportion maps generated by the SPICE algorithm represent the amount of a particular endmember in a pixel, the proportion map associated with the blackbody endmember is used as the blackbody map, v, for the image.

$$v_j = \begin{cases} 0 & if \ E_B = \varnothing \\ p_{jB} & otherwise \end{cases} \tag{21}$$

where j corresponds to the j^{th} pixel in the image. A mask, V, is defined using the blackbody map by inverting the values and enhancing the map using a local 3x3 minimum filter.

$$V_j = localmin(1 - v_j) \tag{22}$$

where j corresponds to the j^{th} pixel in the image. Following the local 3x3 minimum filter, a partial threshold was applied to the mask.

$$V_j^{thresh} = \begin{cases} V_j & if \ V_j < t \\ 1 & otherwise \end{cases} \tag{23}$$

where t is the threshold determined using Otsu's thresholding method. The partial threshold is applied so that the only values modified by the mask are those that are associated with pixels that behave like a blackbody.

3.3 Results

As in reference 1, SPICE was run on a subset of pixels from the image using "candidate points" selected using the Pixel Purity Index (PPI)[9]. The candidate points in our experiments were chosen from 30,000 random projections. Points within a distance of 3 from the boundary of the projection received increased purity indices. In reference 1 , 1000 pixels were used during the experiments on the real image sets. We chose a PPI threshold that allowed us to have as close to 1000 pixels as possible (many pixels have the same PPI). The number of candidate points used was 1095, 767, and 1103 for AHI Images 1, 2, and 3, respectively. After determining the endmembers using the candidate points, the entire image was unmixed using these endmembers to calculate the proportion maps for the entire image.

The results in this paper are compared to those generated using the vegetation mapping method described in reference 7. Since reference 7 uses only the statistics of emissivity (mean, standard deviation and skewness across spectral bands) instead of the full emissivity curve, the results displayed are those generated by running SPICE only of the statistics of emissivity instead of the full emissivity spectra. This was done to be able to compare performance of the clustering method in reference 7 and the SPICE method directly without adding confusion over whether the difference in performance resulted from the methods or the input data. Furthermore, a partial threshold as defined in (23) was also applied the mask generated by the clustering method in reference 7.

In contrast to SPICE, which finds the desired number of endmembers for a data set, the method in reference 7 requires a number of clusters parameter to be set. The method was run on this data with the number of clusters ranging from 3 to 6. The results displayed below are the best results obtained over this range of number of cluster values. Figure 2 shows the blackbody mask generated using SPICE and the clustering method for 4 and 5 clusters. When comparing the two masks generated by the clustering method, it can be seen that when 5 clusters is chosen instead of 4, many of the vegetation pixels are being split between multiple clusters and thus farther from the selected vegetation cluster center. Since SPICE automatically selects the desired number of endmembers, this difficulty is eliminated. When examining the SPICE mask and the Clustering mask generated with 4 clusters, it can be seen that the SPICE mask is more solid and compact thus providing a better masking of the vegetation pixels than the clustering method.

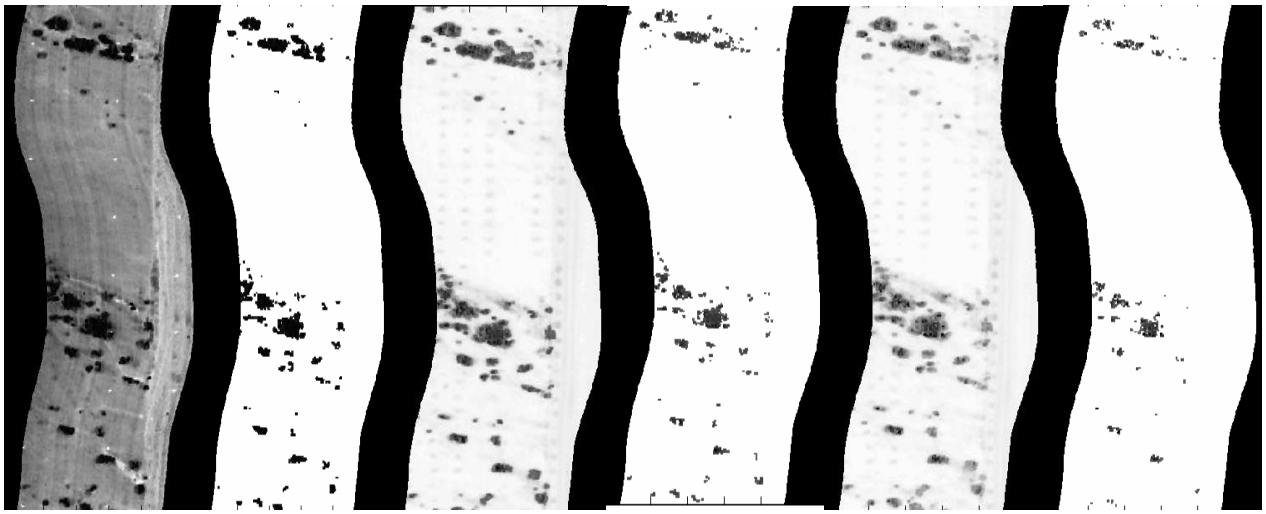

(a) (b) (c) (d) (e) (f)

Figure 2: Blackbody Masks created using SPICE and the Clustering Method. (a) is the blackbody mask generated using SPICE and (b) is the thresholded SPICE mask. (c) is the mask generated using 4 clusters in the clustering method; (d) is the thresholded version of this mask. (e) is the mask generated using 5 clusters in the clustering method and (f) is the thresholded version of this mask.

Points of Interest, POIs, in the overlap regions of the imagery were found using the RX detector algorithm[10]. The RX detector applied is an implementation of the well-known anomaly detection algorithm by Winter[11]. The RX algorithm was applied to detect buried mines in the LWIR hyperspectral imagery. The blackbody mask is incorporated by multiplying the RX confidence of every POI with their corresponding blackbody mask value. This differs from the detection algorithms used in reference 7 where the blackbody mask is applied to the output of a Choquet fusion system incorporating several detection algorithms. In this paper, only the comparative performance of the two blackbody masks are being examined.

The results in each of the three overlap regions are shown in the tables below. The probability of detection, PD, is defined as the number of mines with a confidence above the threshold divided by the total number of mines. The false alarm rate, FAR, is defined as the number of non-mines above the threshold divided by the number of square meters in the overlap region. Although RX was applied to detect buried mines, the results are shown over all mine types in the overlap regions. If detected, fiducial markers in the scene are considered false alarms.

The first line in each table displays the false alarm rates without any blackbody mask being used on the RX values. The second line displays the FARs after applying the blackbody mask generated using the clustering method. The third line shows the reduction in the FAR after using the blackbody mask from the clustering method. The fourth line displays the FAR after applying the blackbody mask generated using SPICE. Finally, the fifth line shows the reduction in FAR after using the blackbody mask from SPICE when compared the results without using a blackbody mask.

Table 2. FAR Reduction using Blackbody Mask in AHI Image 1.

	PD				
	20%	**30%**	**40%**	**50%**	**60%**
RX without BB Mask	2.3e-3	3.3e-3	5.8e-3	6.7e-3	9.0e-3
With Clustering BB Mask 5 Clusters	2.1e-3	3.0e-3	5.3e-3	6.1e-3	8.3e-3
FAR Reduction	**8.7%**	**9.1%**	**8.6%**	**9.0%**	**7.78%**
With SPICE BB Mask	1.0e-3	1.2e-3	2.3e-3	2.8e-3	4.2e-3
FAR Reduction	**56.5%**	**63.6%**	**60.3%**	**58.2%**	**53.3%**

Table 3. FAR Reduction using Blackbody Mask in AHI Image 2.

	PD				
	20%	**30%**	**40%**	**50%**	**60%**
RX without BB Mask	1.7e-3	2.6e-3	3.8e-3	6.1e-3	8.5e-3
With Clustering BB Mask 4 Clusters	1.4e-3	2.2e-3	2.8e-3	4.2e-3	6.1e-3
FAR Reduction	**17.6%**	**15.4%**	**26.3%**	**31.1%**	**28.2%**
With SPICE BB Mask	1.2e-3	1.9e-3	2.5e-3	3.8e-3	5.8e-3
FAR Reduction	**29.4%**	**26.9%**	**34.2%**	**37.7%**	**31.8%**

Table 4. FAR Reduction using Blackbody Mask in AHI Image 3.

	PD				
	20%	**30%**	**40%**	**50%**	**60%**
RX without BB Mask	3.7e-3	5.2e-3	9.2e-3	1.2e-2	1.6e-2
With Clustering BB Mask 3 Clusters	3.7e-3	5.2e-3	9.2e-3	1.2e-2	1.6e-2
FAR Reduction	**0%**	**0%**	**0%**	**0%**	**0%**
With SPICE BB Mask	3.3e-3	4.4e-3	6.8e-3	1.0e-2	1.4e-2
FAR Reduction	**10.8%**	**15.4%**	**26.1%**	**16.7%**	**12.5%**

4. CONCLUSION

The SPICE algorithm extends the ICE algorithm with the addition of a sparsity promoting term. This term encourages the pruning of excess endmembers by penalizing the objective function when a large number of endmembers are being used. The sparsity promoting term drives the set of proportions associated unnecessary endmembers to zero at which point that endmember can be pruned from the set of endmembers representing the data.

As shown in Section 3, the blackbody mask generated using the SPICE algorithm can provide false alarm reduction during landmine detection. In comparison to the clustering method in reference 7, the SPICE method provides improved vegetation detection and eliminates the need to set the number of clusters or endmembers needed.

Although results suggest that the SPICE algorithm removes the need to know the number of endmembers needed for a scene in advance, there are still a number of parameters that need to be set, e.g., the gamma constant and the regularization parameters. Future work can include investigation of methods to automatically set these parameters.

ACKNOWLEDGMENT

Research was sponsored by the U. S. Army Research Office and U. S. Army Research Laboratory and was accomplished under Cooperative Agreement Number DAAD19-02-2-0012. The views and conclusions contained in this document are those of the authors and should not be interpreted as representing the official policies, either expressed or implied, of the Army Research Office, Army Research Laboratory, or the U. S. Government. The U. S. Government is authorized to reproduce and distribute reprints for Government purposes notwithstanding any copyright notation hereon. We'd also like to thank Miranda Schatten for her help and support with data and ideas.

REFERENCES

1. M. Berman, H. Kiiveri, R. Lagerstrom, A. Ernst, R. Donne and J. F. Huntington, "ICE: A Statistical Approach to Identifying Endmembers in Hyperspectral Images," *IEEE Trans. On Geoscience and Remote Sensing*, vol. 42, Oct. 2004, pp. 2085–2095.
2. P. Williams, "Bayesian Regularization and Pruning Using a Laplace Prior," *Neural Computation*, vol. 7, pp. 117-143, 1995.
3. M. A. T. Figueiredo, "Adaptive Sparseness for Supervised Learning," *IEEE Trans. On Pattern Analysis and Machine Intelligence*, vol. 25, Sept. 2003, pp. 1150–1159.
4. P.G. Lucey, T.J. Williams, M. Mignard, J. Julian, D. Kobubun, G. Allen, D. Hampton, W. Schaff, M. J. Schlangen, E. M. Winter, W. B. Kendall, A. D. Stocker, K. A. Horton, A. P Bowman, "AHI: An Airborne Long-Wave Infrared Hyperspectral Imager", *Proc. of SPIE,* Vol. 3431, Nov. 1998, pp 36-43.
5. General Atomics, *LYNXSAR*, [Online]. Available: http://www.LYNXSAR.com
6. A. N. French, T. J. Schmugge, and W. P. Kustas, "Discrimination of Senescent Vegetation Using Thermal Emissivity Contrast," *Remote Sensing of Environment*, Vol. 74, pp. 249-254, 2000.
7. A. Zare, J. Bolton, P. Gader, and M. Schatten, "Vegetation Mapping for Landmine Detection Using Long Wave Hyperspectral Imagery," *IEEE Trans. Geoscience and Remote Sensing*, Paper Submitted.
8. P. Kealy and S. Hook, "Separating Temperature and Emissivity in Thermal Infrared Multispectral Scanner Data: Implications for Recovering Land Surface Temperatures," *IEEE Trans. Geoscience and Remote Sensing*, Vol. 21, No. 10, pp. 2127-2132, 2000.
9. Winter, M. E., "Fast Autonomous Spectral End-member Determination In Hyperspectral Data", *Proceedings of the Thirteenth International Conference on Applied Geologic Remote Sensing*, Vol. II, Vancouver, B.C., Canada, 1999, pp 337-344.
10. X. Yu, I. S. Reed, and A. D. Stocker, "Comparitive Performance Analysis of Adaptive Multispectral Detectors," *IEEE Trans. Signal Processing*, Vol. 41, No. 8, Aug. 1993, pp. 2639-2656.
11. E. Winter, Personal Communication.